Available online at www.sciencedirect.com
ScienceDirect
Journal of the European Ceramic Society 27 (2007) 4719–4725
www.elsevier.com/locate/jeurceramsoc

Elasticity and lattice vibrational properties of transparent polycrystalline yttrium–aluminium garnet: Experiments and pair potential calculations

P. Djemia [a,*], F. Tétard [a], K. Bouamama [b], Eric Charron [c], D. Tétard [d], Y. Rabinovitch [d,e]

[a] *Laboratoire des Propriétés Mécaniques et Thermodynamiques des Matériaux, UPR CNRS 9001, Université Paris Nord, 99 Avenue J.B. Clément, 93430 Villetaneuse, France*
[b] *Département de Physique, Université Ferhat Abbas, Sétif 19000, Algeria*
[c] *Institut des Nanosciences de Paris, UMR CNRS 7588, Campus boucicaut, 140 rue de Lourmel, 75015 Paris, France*
[d] *Sciences des Procédés Céramiques et des Traitements de Surfaces, UMR 6638, Faculté des Sciences de Limoges, 123 Avenue Albert Thomas, 87060 Limoges Cedex, France*
[e] *CILAS Limoges, Bâtiment ESTER B.P. 76923, 87069 Limoges Cedex, France*

Received 13 December 2006; received in revised form 7 February 2007; accepted 23 February 2007
Available online 18 April 2007

Abstract

Brillouin light scattering, Raman light scattering and visible–infrared reflectometry techniques have been used to investigate, respectively, the elastic properties, the phonons and the optical properties of bulk textured polycrystalline yttrium–aluminum garnet doped with 2 at% neodymium obtained by the sintering of commercial oxides. From the analysis of the observed bulk longitudinal and transverse acoustic modes with the knowledge of the refractive index 1.81 inferred from the visible reflectometry, the two independent effective elastic constants of the isotropic polycrystal $C_{11} = 362$ GPa and $(C_{11} - C_{12})/2 = 121$ GPa are determined leading to the value of the bulk modulus $B = (C_{11} + 2C_{12})/3 = 200$ GPa. The ratio $\varepsilon_0/\varepsilon_\infty = 3.1$ and the optic permittivity $\varepsilon_\infty = 3.46$ are derived from the infrared reflectivity data. Pair potential calculations of the three single crystal elastic constants $c_{11} = 340$, $c_{12} = 127$ and $c_{44} = 112$ GPa, of the bulk modulus $B = (c_{11} + 2c_{12})/3 = 198$ GPa, of the zone-center (Γ) phonons and of the permittivity function provide good comparison with our experimental results.

Keywords: Sintering; Dielectric properties; Mechanical properties; Optical properties; Pair potential calculations

1. Introduction

The determination of the elastic and optical properties of materials is important for both physical models and engineering application purposes. Yttrium aluminum garnet $Y_3Al_5O_{12}$ (YAG) is of high technological interest either under ceramics or single crystal form. YAG is host of neodymium dopants in solid state laser. It crystallizes in a cubic $Ia3d$ (O_h^{10}) structure with eight formulae per unit cell (160 atoms). The cations are all in special positions: labeled as a, c, and d with no positional degrees of freedom whereas the O atoms are placed in the general positions 96(h). Y occupies dodecahedral 24(c) positions, whereas there are two different sites for Al ions: namely, octahedral 16 (a) and tetrahedral 24 (d) in the lattice.

Since Coble,[1] as the first one, produced transparent alumina ceramics, other teams have developed new polycrystalline materials for optical applications. For example transparent polycrystals have been synthesized for electro-optical utilization[2] or as laser amplifying media. For this last function, only few compounds in transparent ceramic form have been successfully tested in a laser cavity.[3–7] Neodymium-doped YAG is one of the best known single crystal laser materials. It is used for various industrial or medical purposes. Because of its good thermal conductivity of about 10 W/m K although a single crystal alumina has about 30 W/m K, it is a good candidate for powerful applications such as inertial fusion, or for military devices. Yet, the maximum size of good quality YAG single crystals for optical applications does not exceed 18 cm in length and 2 cm in

* Corresponding author. Tel.: +33 149403482; fax: +33 149403938.
E-mail address: djemia@lpmtm.univ-paris13.fr (P. Djemia).

0955-2219/$ – see front matter © 2007 Elsevier Ltd. All rights reserved.
doi:10.1016/j.jeurceramsoc.2007.02.216

diameter. In polycrystalline form, there is theoretically no size limitation. Undoped YAG translucent ceramics have been produced by de With et al.,[8] and Nd-doped polycrystalline YAG by Sekita et al.[9] Major work on the subject has been provided by teams of Ikesue and Konoshima Chemicals.[10] Recently, Rabinovitch et al.[7] have demonstrated that high transparency and laser efficient polycrystalline YAG:Nd can be synthesized by sintering of commercial oxides. We used one of their polycrystalline sample in this study, with 2 at% Nd doping.

To better understand the intrinsic properties of polycrystalline YAG, we have studied in detail some structural, mechanical and vibrational aspects of this isotropic polycrystalline sample. Previous Brillouin light scattering (BLS) or acoustic studies dealt with single crystal and measurements of high temperature or pressure dependant elastic properties associated with refractive index measurements.[11–14] In this paper, the elastic, the dielectric and vibration properties of polycrystalline samples are studied in relation with the crystallographic texture. The experimental investigations have been carried out using X-ray diffraction, Raman scattering, infrared–visible reflectometry with oblique incidence and the BLS technique which has proved to be a powerful nondestructive tool for the elastic characterization of layered structures and bulk materials.[15] The two independent elastic constants of the isotropic samples are selectively determined from the analysis of a longitudinal and a transversal acoustic modes traveling nearly parallel to the normal of the samples. The calculated Voigt and Reuss average[16] values of the effective elastic constants for an isotropic polycrystal using the pair potential calculated single crystal elastic constants are compared to the ones derived from the analysis of our BLS experiments. The vibrational features are also compared to the pair potential calculations.

2. Light scattering techniques and infrared reflectometry

In a BLS experiment, a beam of monochromatic light is used as a probe to reveal acoustic phonons that are naturally present in the medium under investigation. The power spectrum of these excitations is mapped out from frequency analysis of the light scattered within a solid angle, by means of a multipass Fabry–Perot interferometer. Several scattering geometry can be used and a number of acoustic modes in the material can thus be revealed, and the elastic constants determined.[17–20]

In the present work we used the backscattering geometry. In this condition the wave vector of the involved bulk phonons Q_B is experimentally adjusted to the value:

$$Q_B = 2nk_I \quad (1)$$

where n is the refractive index of the material corresponding to the propagation direction of light inside the film (isotropic for materials of cubic symmetry), k_I the optical wave vector in air. The velocity v_B is deduced from the measured frequency Ω by the relation:

$$v_B = \frac{\Omega}{Q_B} \quad (2)$$

Due to refraction at the air/sample interface, the bulk waves associated with the bulk longitudinal wave (BLW) and the bulk shear waves (BSW) have a wave vector inside the material at an angle:

$$\alpha = \sin^{-1}\left(\frac{\sin(i)}{n}\right) \quad (3)$$

from the normal of the sample where i is the angle of incidence of light.

The Brillouin experiments were performed at room temperature. The light source is an Ar^+ laser tuned on a 514.5 nm single mode line. Incident 100–500 mW p-polarized light is focused inside the sample. The scattered light is analyzed by means of a Sandercock-type 3 + 3 pass tandem Fabry–Perot interferometer. The typical duration for the acquisition of a Brillouin spectrum was 10 min.

The FTIR reflectance spectra were recorded using a Perkin-Elmer GX spectrometer at a resolution of 2 cm^{-1} with a spectral range of 370–10,000 cm^{-1}, at an angle of incidence of 30°. All IR spectra were the results of the averaging of 200 scans. Raman spectra have been obtained with a triple monochromator micro-Raman *DILOR XY* multichannel spectrometer equipped with nitrogen cooled CCD detector (Jobin Yvon) using less than 100 mW green light.

3. Samples preparation and structural characterizations

In this process commercial oxides are used. Alumina, yttrium oxide (Alfa Aesar, 99.99%), neodymium oxide (reacton, 99.99%) are weighed in order to obtain the compound $Nd_xY_{1-x}Al_5O_{12}$ (Nd doped YAG) where x is the atomic substitution of yttrium by neodymium. Silica (Alfa Aesar, 99.8%) is added as sintering aid. Silica forms liquid phases above 1600 °C with Nd_2O_3 and 1660 °C with Y_2O_3. Even if very small amounts of silica are introduced in the sample, it is believed that these liquid phases soak the grain boundaries. Indeed, scanning electron microscopy (SEM) analyses[7] have shown that the grain boundaries contain more yttrium and neodymium than the bulk of the samples. The amount of silica added in our samples is 500 ppm in weight and the neodymium atomic substitution rate is 2 at%.

The mean particle sizes are 1.1, 0.8, 6 μm and 10 nm for Al_2O_3, Y_2O_3, Nd_2O_3 and SiO_2, respectively. The powders are mixed in water. The mixture is then dried or used directly for axial or isostatic pressing between 200 and 300 MPa. The compacted powders are then sintered at 1700 °C for 3 h under vacuum. The density of the ceramics measured by Archimede method was 4.56 ± 0.02 g/cm^3. The microstructure of sintered samples is shown in Fig. 1. The average grain length estimated by an image analysis software is about 7 μm. Porosity and secondary phases were not detected in our samples by SEM, because of very few amount of defects which were estimated below 0.1 vol.%. X-ray diffraction using a copper anode (see Fig. 2) shows diffraction features comparable to those of a powder (JCPDS Card No. 33–40) indicating no preferential crystallographic orientation normal to the film plane, a value of the cell parameter 12.006 ± 0.006 Å and a value of the mass den-

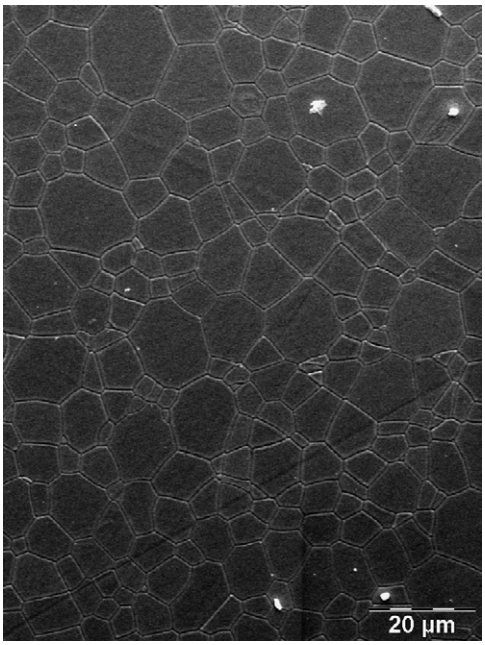

Fig. 1. Microstructure SEM observation of a YAG:Nd 2 at% polycrystalline sample sintered at 1700 °C for 3 h under vacuum.

sity 4.561 g cm^{-3}. Thus the sample will be considered later as an isotropic polycristal. In the literature, it has been shown that secondary phases could appear during YAG sintering. This is the case when a too large amount of silica is added.[21] Moreover alumina precipitates have been observed at the grain boundaries or in grains as inclusions.[22]

Phases rich in yttrium and silica occur frequently when silica content is generally above 1500 ppm in conventional transparent YAG ceramics.[23] In our case, the silica content was sufficiently low to overcome this problem. Concerning alumina precipitates, our process was finalized to avoid their formation, especially by controlling the oxygen partial pressure in kiln atmosphere during annealing stage of the ceramics at 1400 °C.

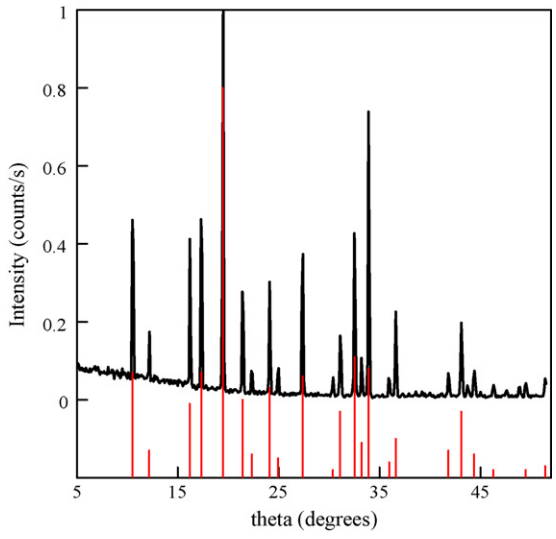

Fig. 2. X-ray diffraction spectrum of the polycrystalline YAG:Nd with Cu Kα_1 radiation compared to the spectrum of a powder (from JCPDS Card No. 33–40).

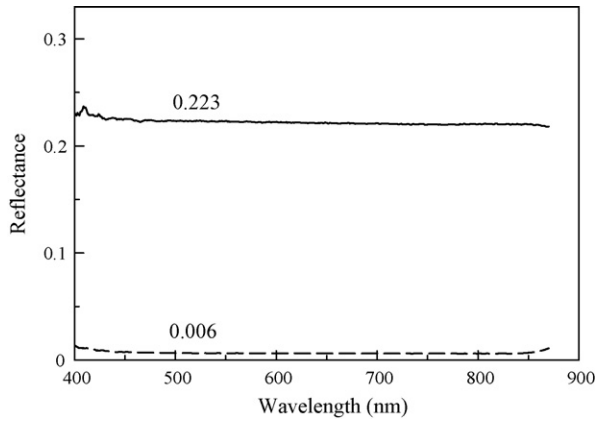

Fig. 3. Visible reflectometry spectra for an angle of incidence of 55° and p-polarization (dashed line) or s-polarization (line) of the incident light.

Visible reflectometry with an angle of incidence ranging from 30 to 60° with p- and s-polarization of the incident light were performed (see Fig. 3). The material does not show significant dispersion of the refractive index with the wavelength and is highly transparent. The analysis for both polarization provides the value of the refractive index $n = 1.81$. These properties combined with its high laser efficiency[7] confers to this material a high potentiality.

4. Results and discussion

The bulk acoustical waves observed in the Brillouin spectra have been analyzed considering an isotropic elastic symmetry of the polycrystalline sample that is confirmed by the observation of identical results for various experiments with different angle of incidence of the light that probe different wave propagation direction within the sample.

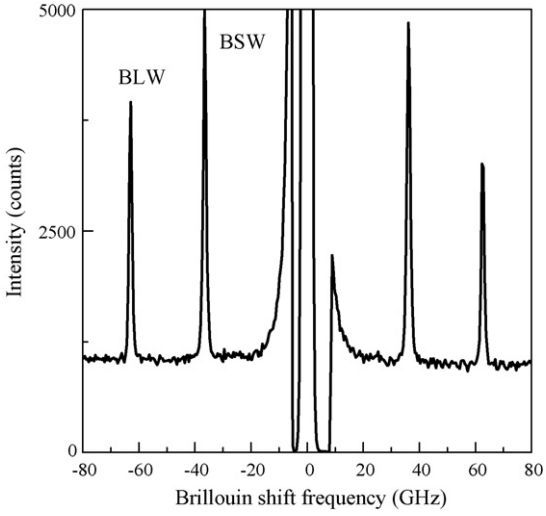

Fig. 4. Experimental Brillouin spectrum obtained (p incident light – np scattered light geometry) at high frequency with an angle of incidence $i = 65°$ corresponding to $\alpha = 30°$. The peaks labeled BSW and BLW correspond, respectively, to the bulk shear acoustic wave and to the bulk longitudinal acoustic wave. The background comes from the luminescence.

Table 1
Measured velocity v of the bulk acoustic waves and their related elastic constants ρv^2 (the mass density is assumed to be 4.561 g/cm^3 from X-ray measurements. Other experimental or calculated results are reported for comparison

Sample	v_{BSW} (m/s)	v_{BLW} (m/s)	C_{44} (GPa)	C_{11} (GPa)	E (Gpa)	ν	B (Gpa)	a (Å)	ρ (g cm^{-3})
Polycrystal (this work)	5155 ± 25	8905 ± 40	121 ± 1	362 ± 3	302 ± 3	0.248 ± 0.002	200 ± 2	12.006 ± 0.006	4.561
Voigt or Reuss	4910	8685	110	344	297	0.229	198		

	v_{BSW} (m/s)	v_{BLW} (m/s)	c_{44}	c_{12}	c_{11}	B (Gpa)	ρ (g cm^{-3})
Single crystal							
Stoddart et al.[11]			116	114	339	189	
Chistyi et al.[12]			114	114	333	187	
Yogurtçu et al.[13]	4940	8490	114	106	328	180	4.55

The Voigt or Reuss estimated values of the elastic constants for the isotropic textured polycrystalline sample using for calculations the calculated single crystal values from Kukjla et al. potential[26] are also reported for comparison below our experimental results.

In Fig. 4, we show a spectrum for an angle of incidence $i = 45°$ with no polarization of the analyzed scattered electric field. The peaks labeled BSW and BLW correspond, respectively, to the bulk shear wave and the bulk longitudinal wave traveling nearly parallel to the film normal.

The measurements of the frequency position of these Brillouin peaks and the knowledge of the refractive index $n = 1.81$ determined by visible reflectometry, provide the phase velocity v of the corresponding acoustic modes, according to Eqs. (1) and (2). Notice that the phase velocity of the BLW is $\sqrt{C_{11}/\rho}$ and that of BSW is $\sqrt{(C_{11} - C_{12})/2\rho}$, so that C_{11} and $C_{44} = (C_{11} - C_{12})/2$ can be directly determined using $\rho = 4.561$ g/cm^3 for the mass density as calculated from unit cell contents and constant (conform Fig. 2.). The measured velocity data are reported in Table 1 with their related elastic constants. The elastic moduli and the Poisson's coefficient can be calculated through well-known relations.[24] The value of the Young modulus E and of the Poisson ratio ν are, respectively, 302 GPa and 0.248 while the bulk modulus is $B = (C_{11} + 2C_{12})/3 = 200$ GPa.

As a further step in estimating the elastic properties and the dielectric properties of YAG, neglecting the 2 at% Nd doping of our sample, we have performed pair potential calculations using the GULP software written by Gale.[25] We used a pair potential that is adapted to ionic materials with Kukjla,[26] Bush[27] or Schuh[28] parameters for the Buckingham potential[29] Eq. (4) with parameters (A, ρ and C) that are reported in,Ref. [26–29] instead of the Born–Mayer potential that was used by Papagelis et al.[30]

$$\Psi(r) = A \exp\left(-\frac{r}{\rho}\right) - Cr^{-6} \quad (4)$$

Accurate representation of the ionic polarization of the crystalline lattice was shown to be very important for defect modeling and description of optical properties of YAG.[26] Therefore, we have considered all the constituent ions of YAG (i.e.,Y^{3+}, Al^{3+}, and O^{2-}) as being polarizable ions in the lattice adding three spring core-shell parameters[26] (K^+) to the description of the crystal lattice energy. For calculations, before optimization of the structure, our experimental unit cell parameter 12.006 Å is considered and the O positional parameters in the lattice were taken from neutron-diffraction measurements by Prince[31] and are given by $x = -0.029$, $y = 0.053$, and $z = 0.151$. The structural optimization that minimizes the energy leads to a final unit cell constant of 11.988 Å and new O positional parameters in the lattice: $x = -0.023$, $y = 0.055$, and $z = 0.154$ (O core) and $x = -0.025$, $y = 0.0519$, and $z = 0.155$ (O shell). The calculations are made for this optimum structure. Whereas Geller,[32] determined the most accurate value of the lattice constant for the stoichiometric YAG that is 12.000 ± 0.002 Å, several other experimental studies have determined the lattice constant to be slightly higher (we found 12.006 ± 0.006 Å), which may be due to the presence of excess yttrium in the lattice.[32]

We calculated the elastic constants, the dielectric properties and phonons at the Γ point, the parameters from Kukjla et al.[26] leading definitely to the best agreement with the overall experimental results (structural, elastic and dielectric properties). The elastic constant matrix has been calculated from second derivative of the energy density with respect to external strain. Due to the cubic symmetry of garnet structures, the elastic constant matrix elements that have to be estimated are c_{11}, c_{12}, and c_{44}. The values of elastic constants and the bulk modulus $B = (c_{11} + 2c_{12})/3$ so derived are summarized in Table 2. These calculated single crystal constants are in fairly good agreement

Table 2
Pair potential calculations of structural (a, ρ) and elastic properties (c_{44}, c_{12}, c_{11} and B) to be compared to the experimental results of Table 1

	c_{44} (GPa)	c_{12} (GPa)	c_{11} (GPa)	B (Gpa)	a (Å)	ρ (g cm^{-3})
GULP						
Kuklja et al.[26]	112	127	340	198	11.988	4.58
Bush et al.[27]	131.3	164.6	330.5	220	12.143	4.40
Schuh et al.[28]	117	135	395	221	12.002	4.53
Papagelis et al.[30]	60	102.4	263.3	156		
(Brout's formula) Hofmeister et al. [33]				220		

The bulk modulus calculated from the single crystal constants has to be compared to the polycrystalline one as it is an invariant parameter.

with the experimental determinations and provide a value of the bulk modulus $B = 198$ GPa (Kukjla potential[26] is used for this evaluation) that compares very well with our experimental result (200 GPa). For comparison purpose, the calculated values of the effective elastic constants of non-textured isotropic polycrystalline YAG following a Voigt and Reuss averaging procedure[16] using the calculated single crystal elastic constants with Kukjla potential[26] are also reported in Table 1. It provides close agreement with our elastic constants on a polycrystalline sample and with a bulk modulus value that is the same for the single crystal and the polycrystalline estimations.

Next, we discuss the dielectric and elastic properties derived from infrared and Raman scattering. The 240 degrees of freedom of the rare earth aluminium garnets can be classified for the BZ center according to the irreducible representations of the O_h group as follows: $\Gamma = 18T_{1u} + 3A_{1g} + 8E_g + 14T_{2g} + 5A_{2g} + 5A_{1u} + 5A_{2u} + 10E_u + 14T_{1g} + 16T_{2u}$. For the garnet structure a large number of zone center modes are silent ($5A_{2g}$, $5A_{1u}$, $5A_{2u}$, $10E_u$, $14T_{1g}$, $16T_{2u}$) and have not been investigated through inelastic neutron measurements so far. The 25 modes having symmetries A_{1g}, E_g and T_{2g} are Raman active while the 18 having T_{1u} symmetry are IR active. Most of these peaks are observed in Raman and infrared spectra (see Fig. 5). The knowledge of the zone center phonon frequencies : mainly, IR and Raman frequencies, along with the structural parameters can be exploited for an adequate estimation of the elastic properties of cubic crystals.[33] According to this model[33] which is a generalization of Brout's formulation for diatomic cubic crystals for any cubic solid,[34] the bulk modulus of the garnet crystal can be estimated to 220 GPa[35] that is 10% higher to both our experimental and calculated determination (see Tables 1 and 2).

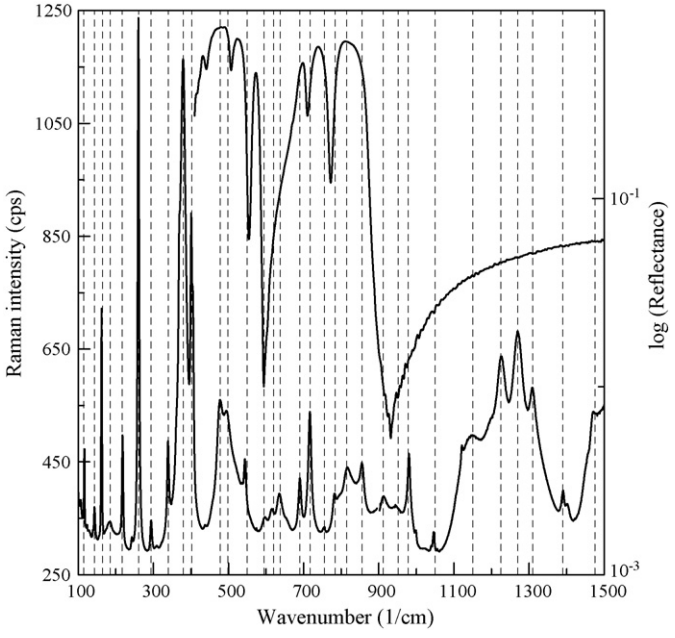

Fig. 5. Comparison of a micro-Raman spectrum (green incident light with 150 mW power) with an infrared reflectometry spectrum (30 incidence). (For interpretation of the references to colour in this figure legend, the reader is referred to the web version of the article.)

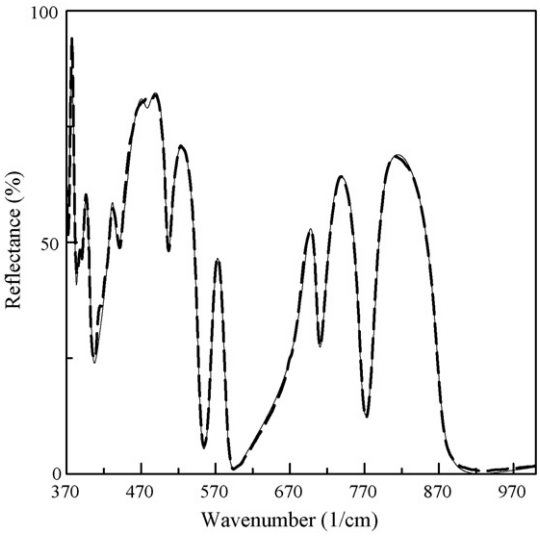

Fig. 6. Experimental (dashed line) and calculated (line) infrared reflectometry spectrum with an angle of incidence of 30° and no polarization of the incident light.

The frequency of TO and LO T_{1u} modes can be determined from reflection spectra using a multi-oscillator analysis or from a direct Kramers–Konig transformation of the reflectance spectra. We performed both analysis. The best fit of the factorized form of the dielectric function Eq. (5) to our reflectivity data is shown in Fig. 6. The incident light is not polarized and the angle of incidence is 30°.

$$\varepsilon(\omega) = \varepsilon_\infty \prod_k \frac{\omega_{kLO}^2 - \omega^2 + i\gamma_{kLO}\omega}{\omega_{kTO}^2 - \omega^2 + i\gamma_{kTO}\omega} \tag{5}$$

The fitting parameters: frequencies and line widths of both transverse optical (TO) and longitudinal optical (LO) modes are given in Table 3. The oscillator strengths of the modes, in other words the contribution of the polar modes to the dielectric constant, are also given in Table 3. Oscillator strengths $\Delta\varepsilon_j$ are not adjustable parameters in this model. They are calculated from the splitting of polar modes into TO and LO components with the aid of Eq. (6):

$$\frac{\Delta\varepsilon_j}{\varepsilon_\infty} = \omega_{jTO}^{-2} \frac{\prod_k \left(\omega_{kLO}^{-2}\right) - \left(\omega_{jTO}^{-2}\right)}{\prod_{k\neq j} \left(\omega_{kTO}^{-2}\right) - \left(\omega_{jTO}^{-2}\right)} \tag{6}$$

The static ε_0 and the high frequency ε_∞ dielectric constants are related to the infrared frequencies trough the Lydane–Sachs–Teller (LST) relation[37,38]

$$\frac{\varepsilon_0}{\varepsilon_\infty} = \prod_k \left(\frac{\omega_{kLO}}{\omega_{kTO}}\right)^2 \tag{7}$$

In Table 4 the values for the ratio $\varepsilon_0/\varepsilon_\infty$ are derived from the experimental ω_{LO} and ω_{TO} reported in Table 3. The theoretical values of ε_∞ calculated with the Kukjla potential[26] (3.5) shows 1–7% difference to the ones obtained independently from measurements of the refractive index in the visible region (3.27), from the Kramers–Kronig analysis (see Fig. 7) of the FTIR

Table 3
IR optical modes frequencies and damping factors as inferred from the best fit of the oblique incidence reflectivity spectrum using a factorized form of the permittivity function (see the text)

Mode number k	ω_{kTO} (cm^{-1})	γ_{kTO} (cm^{-1})	ω_{kLO} (cm^{-1})	γ_{kLO} (cm^{-1})	$\Delta\varepsilon_k$
1[a]	122.3 (130)	4.5	122.6 (136.9)	4.5	0.06
2[a]	164.5 (164)	4.6	173.4 (169.2)	2.8	1.35
3[a]	178.8 (186)	2.0	180.0 (188)	2.0	0.06
4[a]	219.9 (246)	4.0	224.5 (255.9)	4.0	0.42
5[a]	290.6 (294.1)	3.7	295.7 (300.5)	3.7	0.49
6[a]	329.4 (312)	5.5	338.4 (314)	5.5	0.72
7	375.4 (336)	1.2	381.5 (352.4)	4.3	0.72
8	386.6 (353.9)	7.2	389.5 (365.1)	6.9	0.22
9	393.7 (380.1)	6.5	403.3 (415.6)	10.0	0.30
10	430.0 (419.2)	7.6	434.9 (422)	14.0	0.40
11	453.9 (442)	20.0	477.0 (476.2)	14.0	1.48
12	478.0 (508)	15.0	504.8 (516)	11.0	0.05
13	509.3 (518)	14.0	547.8 (563)	10.4	0.09
14	565.7 (572)	9.0	583.4 (600.1)	9.8	0.07
15	693.0 (608)	16.0	707.3 (633.1)	11.0	0.40
16	720.7	17.5	765.8	15.3	0.29
17	785.3	15.4	860.5	17.3	0.12

The optic permittivity is $\varepsilon_\infty = 3.46$ and the oscillator strength $\Delta\varepsilon_k$ is calculated from the splitting of TO and LO modes (see the text).
[a] Are the results from Le Floch et al.[36] below 370 cm^{-1}. The frequencies of TO and LO modes that have been obtained from the maximum or the zero, respectively, of the calculated real part of the permittivity function with GULP program and kukjla et al. potential (see Fig. 8) are indicated in parenthesis.

Table 4
The ratio $\varepsilon_0/\varepsilon_\infty$ derived from the LST relation by using the experimental values of the ω_{TO} and ω_{LO} frequencies

Calculations (GULP)				Experiments			
Potential	$\varepsilon_0/\varepsilon_\infty$	ε_∞	ε_0	LST $\varepsilon_0/\varepsilon_\infty$	KK ε_∞	n^2	ε_∞
Kuklja et al.[26]	3.26	3.5	11.4	3.10	3.61 ± 0.3	3.27 ± 0.01	3.46 ± 0.03
Bush et al .[27]	4.08	3.96	16.15				
Schuh et al.[28]	2.79	2.9	8.1				

The value of ε_∞, inferred from the Kramers–Kronig analysis of the reflectivity spectrum is also given. The refractive index n is derived from the visible reflectivity experiments and nearly constant in the entire range of wavelength. ε_∞ is also obtained from the best fit of reflectivity data using the factorized form of the permittivity function (last column).

reflectance spectrum at high frequency (3.61) or from the best fit of the reflectivity data using the factorized form Eq. (5) of the permittivity function (3.46). The theoretical frequencies of phonons reported in Table 3 are derived from the analysis of the calculated real part of the permittivity function with the GULP program (see Fig. 8), in the range 50–900 cm^{-1}, with a damping factor and a frequency step of 2 cm^{-1}. In Fig. 8, we compare this theoretical function to the factorized form of Eq. (5): the TO modes frequencies are given by the maxima and the LO modes frequencies by the zero. The comparison is qualitative and some modes are missing at higher frequency.

Our experimental results are in agreement with previous determinations in single crystal or polycrystalline samples.[30,35,39] For Y garnets, a value around 10 is found for ε_0[35], which seems to be correct also in the case of aluminum garnets, if we consider our experimental $\varepsilon_0/\varepsilon_\infty \sim 3.1$ ratio values. The difference between the optic and static dielec-

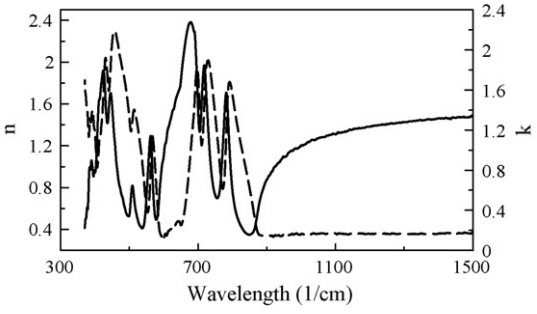

Fig. 7. Refraction index (real part: line, imaginary part: dashed line) in the infrared region obtain from the Kramers–Konig transformation of the experimental reflectance spectrum of Fig. 5.

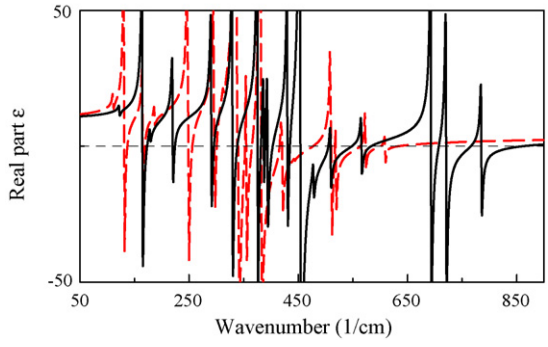

Fig. 8. Real part of the permittivity function in the infrared region: factorized form (line) and GULP calculation (dashed line). The frequencies of TO and LO modes can be obtain from the maximum or the zero, respectively.

tric constants $(\varepsilon_0/\varepsilon_\infty) \sim 7$ indicates a rather mixed character in the bond strengths of the whole crystal class. This has to be attributed to the presence of various types of bonds and to the strongly coupled polyhedra present in the garnet structure.

5. Summary and conclusion

We have determined using Brillouin light scattering the elastic properties of a transparent isotropic textured polycrystalline yttrium-aluminum oxyde made by the sintering of commercial oxides. The two independent effective elastic constants of the isotropic textured polycrystalline crystal have been successfully measured. The two elastic constants of the polycrystalline sample C_{11} and C_{44} were obtained from measurements of the phase velocity of the bulk longitudinal and of the shear horizontal modes. The single crystal elastic constants c_{11}, c_{12} and c_{44} constants, the static and optic permittivity and phonons frequencies at the zone-center were calculated with the GULP software[25] using 3 different available pair potentials.[26–28] The calculated single crystal elastic constants were used as input for the calculation of the Voigt and Reuss[16] averages for our isotropic cubic polycrystalline sample. A fairly good agreement was found with our experimental results. The dielectric properties ε_∞ and $\varepsilon_0/\varepsilon_\infty$ were determined from the Lyddane–Sachs–Teller relation using experimental frequencies from IR measurements. Semi-empirical relations of vibrational data with macroscopic properties, such as that of LST and of Brout's formula for bulk modulus, were found to be in reasonably good agreement with both experimental values and pair potential calculations. It demonstrates that the sintering of commercial oxides can be used to synthesized extremely good quality transparent polycrystalline YAG ceramic for technical purposes.

References

1. Coble, R.L., US Patent 3,026,210 (1962).
2. Heartling, G. H. and Land, C. E., Hot-pressed (Pb,La)(Zr,Ti)O_3 ferroelectric ceramics for electrooptic applications. *J. Am. Ceram. Soc.*, 1971, **54**(1), 1–10.
3. Carnall, E., Jr., Hatch, S.E., Parsons, W.F., FR Patent 1448145 (1966).
4. Greskovich, C. and Chernoch, J. P., Polycrystalline ceramic lasers. *J. Appl. Phys.*, 1973, **44**(10), 4599–4606.
5. Lu, Ji., Lu, Ju., Murai, T., Takaichi, K., Uematsu, T., Ueda, K.-I. *et al.*, Nd^{3+}:Y_2O_3 ceramic laser. *Jpn. J. Appl. Phys.*, 2001, **40**(12A), L1277–L1279.
6. Ikesue, A., Kinoshita, T., Kamata, K. and Yoshida, K., Fabrication and optical properties of high-performance polycrystalline Nd:YAG ceramics for solid-state lasers. *J. Am. Ceramic Soc.*, 1995, **78**(4), 1033–1040.
7. Rabinovitch, Y., Tétard, D., Faucher, M. D. and Pham-Thi, M., Transparent polycrystalline neodimium doped YAG: synthesis parameters, laser efficiency. *Opt. Mater.*, 2003, **24**, 345–351;
   Rabinovitch, Y., Karolak, F., Bogicevic, C., Tétard, D., Dammak, H.B.H., Parent Cooperation Treaty Application No. WO 2005/100281 A1, 2005.
8. de, G., Van Dijk, H.J., FR Patent 2545272 (1984);
   de With, G. and van Dijk, H. J. A., Translucent $Y_3Al_5O_{12}$ ceramics. *Mater. Res. Bull.*, 1984, **19**, 1669–1674.
9. Sekita, M., Haneda, H., Yanagitani, T. and Shirasaki, S., Induced emission cross section of Nd:$Y_3Al_5O_{12}$ ceramics. *J. Appl. Phys.*, 1990, **67**(1), 453–458.
10. Ikesue, A., JP Patent 03-218963 (1991).
11. Stoddart, P. R., Ngoepe, P. E., Mjwara, P. M., Comins, J. D. and Saunders, G. A., High-temperature elastic constants of yttrium aluminum garnet. *J. Appl. Phys.*, 1993, **73**, 7298–7301.
12. Chistyi, I. L., Kitaeva, V. F., Osiko, V. V., Sobolev, N. N., Starikov, B. P. and Timoschechkin, M. I., *Sov. Phys. Solid State*, 1975, **17**, 922;
    Kitaeva, V. F., Zharikov, E. V. and Chistyi, I. L., The properties of crystals with garnet structure. *Phys. Status Solidi A*, 1985, **92**, 475–488.
13. Yogurtçu, Y. K., Miller, A. J. and Saunders, G. A., Elastic behaviour of YAG under pressure. *J. Phys. C: Solid St. Phys.*, 1980, **13**, 6585–6597.
14. Catlow, C. R. A., Comins, J. D., Germano, F. A., Harley, R. T. and Hayes, W., *J. Phys. C*, 1978, **11**, 3197.
15. Nizzoli, F. and Sandercock, J. R., In *Dynamical properties of Solids*, ed. G. K. Horton and A. A. Maradudin. Elsevier Science B.V., 1990.
16. Musgrave, M. J. P., *Crystal acoustics*. Holden Day, San Francisco, 1970.
17. Grimsditch, M. H. and Ramdas, A. K., Brillouin scattering in diamond. *Phys. Rev. B.*, 1975, **11**(8), 3139–3148.
18. Vacher, R. and Boyer, L., Brillouin scattering: a tool for the measurement of elastic and photoelastic constants. *Phys. Rev. B.*, 1972, **6**, 639–673.
19. Djemia, P., Dugautier, C., Chauveau, T., De Barros, M. I. and Vandenbulcke, L., Mechanical properties of diamond films: a comparative study of polycrystalline and smooth fine-grained diamonds by Brillouin light scattering. *J. Appl. Phys.*, 2001, **90**(8), 3771–3779.
20. Moch, P., Djemia, P. and Ganot, F., Un outil pour l'étude des propriétés élastiques des couches et multicouches minces: la spectroscopie Brillouin. *Vide*, 2001, **301**, 565–580.
21. Wen, L., Sun, X., Xiu, Z., Chen, S. and Tsai, C.-T., *J. Eur. Ceram. Soc.*, 2004, **24**(9), 2681–2688.
22. Mulder, C. A. M. and de With, G., *Solid State Ionics*, 1985, **16**, 81–86.
23. Sallé, C., Maître, A., Baumard, J.-F., Rabinovitch, Y., Opt. Rev., submitted.
24. Nye, J. F., Physical properties of crystals. *Chapter VIII*. Clarendon, Oxford, 1957.
25. Gale, J., The General Utility Lattice Program, GULP. Nanochemistry Research Institute, Curtin University of Technology, P.O. Box U1987, Perth 6845, Western Australia. j.gale@curtin.edu.au.
26. Kuklja, M. M. and Pandey, R., Atomistic modeling of native point defects in yttrium aluminum garnet crystals. *J. Am. Ceram. Soc.*, 1999, **82**, 2881–2886.
27. Bush, T. S., Gale, J. D., Catlow, C. R. A. and Battle, P. D., Self-consistent interatomic potentials for the simulation of binary and ternary oxides. *J. Mater. Chem.*, 1994, **4**, 831–837.
28. Schuh, L., Metselaar, R. and Catlow, C. R. A., *J. Eur. Ceram. Soc.*, 1991, **7**, 67–74.
29. Buckingham, R. A., *Proc. R. Soc., A*, 1938, **168**, 264.
30. Papagelis, K. and Ves, S., Vibrational properties of the rare earth aluminium garnets. *J. Appl. Phys.*, 2003, **94**(10), 6491–6498.
31. Prince, E., Neutron diffraction measurements on yttrium–iron and yttrium–aluminum garnets. *Acta Crystallogr.*, 1957, **10**, 787–788.
32. Geller, S., Crystal chemistry of the garnets. *Z. Kristallogr.*, 1967, **125**, 1–47.
33. Hofmeister, A. M., *J. Geophys. Res.*, 1991, **96**, 16181.
34. Brout, R., Sum rule for lattice vibrations in ionic crystals. *Phys. Rev.*, 1959, **113**, 43–44.
35. Hofmeister, A. M. and Campbell, K. R., Infrared spectroscopy of yttrium aluminum, yttrium gallium, and yttrium iron garnets. *J. Appl. Phys.*, 1992, **72**, 638–646.
36. Le Floch, S., Gervais, M. and Gervais, F., Infrared reflectivity study of the metastable solid solution Y_2O_3–Al_2O_3 on both sides of the yttrium aluminium garnet $Y_3A1_50_{12}$ composition. *Mater. Sci. Eng. B*, 1995, **33**, 217–221.
37. Lyddane, R. H., Sachs, R. G. and Teller, E., On the polar vibrations of alkali halides. *Phys. Rev.*, 1941, **59**, 673–676.
38. Cochran, W. and Cowley, R. A., *J. Phys. Chem. Solids*, 1962, **23**, 447.
39. Hurrell, P., Porto, S. P. S., Chang, I. F., Mitra, S. S. and Bauman, R. P., Optical phonons of aluminium yttrium garnet. *Phys. Rev.*, 1968, **173**, 851–856.